

## Host–Guest Systems

## Supramolecular Organization of Dye Molecules in Zeolite L Channels: Synthesis, Properties, and Composite Materials

Pengpeng Cao,<sup>[a]</sup> Oleg Khorev,<sup>[b]</sup> André Devaux,<sup>[a]</sup> Lucie Sägesser,<sup>[c]</sup> Andreas Kunzmann,<sup>[d]</sup> Achim Ecker,<sup>[c]</sup> Robert Häner,<sup>[b]</sup> Dominik Brühwiler,<sup>[c]</sup> Gion Calzaferri,<sup>\*[b]</sup> and Peter Belser<sup>\*[a]</sup>

**Abstract:** Sequential insertion of different dyes into the 1D channels of zeolite L (ZL) leads to supramolecular sandwich structures and allows the formation of sophisticated antenna composites for light harvesting, transport, and trapping. The synthesis and properties of dye molecules, host materials, composites, and composites embedded in polymer matrices, including two- and three-color antenna systems, are described. Perylene diimide (PDI) dyes are an important class of chromophores and are of great interest for the synthesis of artificial antenna systems. They are especially well suited to advancing our understanding of the structure–transport relationship in ZL because their core fits tightly through the 12-ring channel opening. The substituents at both ends of the PDIs can be varied to a large extent without influencing their electronic absorption and fluorescence spectra. The intercalation/insertion of 17 PDIs, 2 terylenes, and 1 quaternarylene into ZL are compared and their interactions with the inner surface of the ZL nanochannels discussed. ZL crystals

of about 500 nm in size have been used because they meet the criteria that must be respected for the preparation of antenna composites for light harvesting, transport, and trapping. The photostability of dyes is considerably improved by inserting them into the ZL channels because the guests are protected by being confined. Plugging the channel entrances, so that the guests cannot escape into the environment is a prerequisite for achieving long-term stability of composites embedded in an organic matrix. Successful methods to achieve this goal are described. Finally, the embedding of dye–ZL composites in polymer matrices, while maintaining optical transparency, is reported. These results facilitate the rational design of advanced dye–zeolite composite materials and provide powerful tools for further developing and understanding artificial antenna systems, which are among the most fascinating subjects of current photochemistry and photophysics.

## Introduction

Molecules slipping through the 0.71 nm wide channel openings of zeolite L (ZL), which widen to 1.26 nm at their largest extension before closing again in a periodic manner, lose much of their freedom of movement. Movement is essentially reduced to 1D back and forth stumbling, if the length of the molecules approaches or exceeds that of two unit cells (u.c.s). The first conclusion would be that there are no options left for fine-tuning of the characteristic properties of the inserted

guests, and hence, for influencing the properties of the resulting molecule–ZL composites. Experience, however, tells a different story. The diversity of guest–ZL composites exhibiting a large range of properties is impressive.<sup>[1–14]</sup> It emerges from the fact that the variety of molecules that fit into these narrow channels is large, and that confinement favors the formation of sandwich-type structures (Scheme 1), including the possibility for rational stopcock modification.<sup>[1,5,11,15–17]</sup> The size and morphology of the ZL host crystals can be tuned from about 30 nm to several micrometers, and from elongated to disk-shaped.<sup>[18–23]</sup> The composites can be organized into extended ordered structures; thus transferring microscopic qualities to the macroscopic scale.<sup>[24–29]</sup> The luminescence properties of nanosized rare-earth ZL composites can be enormously influenced by plugging the channel entrances with an imidazolium-based stopcock.<sup>[17]</sup> Substitution of some of the charge-compensating potassium cations by imidazolium cations (IMZ<sup>+</sup>) can strongly influence the spectral characteristics of pH-sensitive dyes.<sup>[30]</sup> A simple covalent modification pattern of the inserted dyes allows not only control over the contact distance between the dyes, so that exciton interaction can be switched on and off,<sup>[31–34]</sup> but also influences the environment of neighboring dyes in a sandwich structure. The interaction of a functional group of the guest with the ZL channel is not well

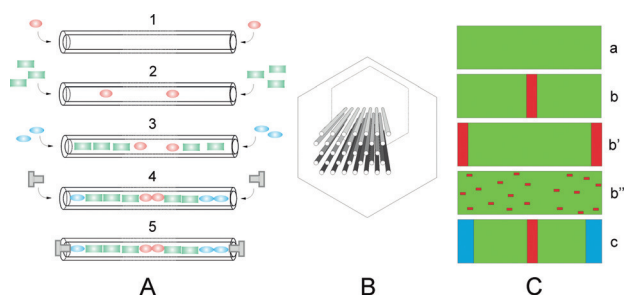
[a] Dr. P. Cao, Dr. A. Devaux, Prof. P. Belser  
Department of Chemistry, University of Fribourg  
Ch. du Musée 9, 1700 Fribourg (Switzerland)  
E-mail: peter.belser@unifr.ch

[b] Dr. O. Khorev, Prof. R. Häner, Prof. G. Calzaferri  
Department of Chemistry and Biochemistry  
University of Bern, Freiestrasse 3, 3012 Bern (Switzerland)

[c] L. Sägesser, Prof. A. Ecker, Dr. D. Brühwiler  
Institute of Chemistry and Biological Chemistry  
Zurich University of Applied Sciences (ZHAW) 8820 Wädenswil (Switzerland)

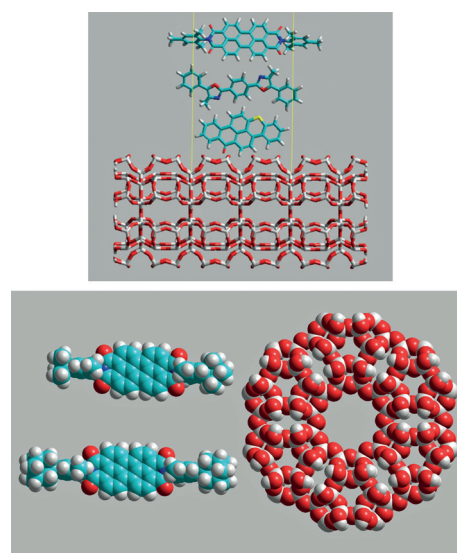
[d] Dr. A. Kunzmann  
Optical Additives GmbH, Flurweg 9  
3073 Gümliigen (Switzerland)

Supporting information and ORCID(s) from the author(s) for this article are available on the WWW under <http://dx.doi.org/10.1002/chem.201504404>.



**Scheme 1.** Synthesis of dye-ZL composites. A) Sequential loading strategy, leading to antenna systems with acceptor dyes in the middle of the channels. B) Schematic view of the hexagonal arrangement of the 1D ZL channels. C) Schematic illustration of different types of dye-ZL composites (D = donor, A = acceptor): a) D-ZL; b) D,A-ZL sandwich, with the acceptor located in the middle of the host; b') A,D-ZL sandwich; b'') random (D,A)-ZL; and c) D1,D2,A-ZL sandwich. The colors indicate the locations of different dyes.

understood. A major exception is the carbonyl group, which binds to the zeolite extra-framework potassium cations, and is thus responsible for dye stabilization in the channels.<sup>[35]</sup> The ZL channels can accommodate more than one type of dye. They can either be loaded one after another, forming a sandwich dye-ZL composite, or simultaneously, leading to a composite containing a random dye mixture. This study focuses on the sandwich-type structure in which different dyes form distinct domains, since the molecules are too large to pass each other inside the channels. This sandwich dye-ZL composite structure has proven to be invaluable for the realization of materials showing efficient Förster resonance energy transfer (FRET)<sup>[36]</sup> antenna characteristics.<sup>[30,37]</sup> We show in Scheme 1C typical patterns, a, b, b', b'', and c, that can be realized by inserting dyes into the channels of hexagonal ZL crystals. Dyes that absorb light at a shorter wavelength are referred to as donors (D), whereas those that absorb light at a longer wavelength as acceptors (A). A system marked as dye-ZL contains only one kind of dye. A composite containing two dyes is referred to as dye<sub>2</sub>,dye<sub>1</sub>-ZL, in which the sequential insertion order is indicated by the ordering of the dye names from right to left. In this case, dye<sub>1</sub> would have been inserted before dye<sub>2</sub>. Crystals of about 500 nm in length and diameter are convenient for many applications and have been chosen because their size meets the criteria that must be respected for the preparation of antenna composites for light harvesting, transport, and trapping. They consist of about 67 000 strictly parallel channels, each of which is formed by 666 u.c.s of 0.75 nm in length. There is space in each channel for a maximum of 333, 222, or 200 molecules of HR, DMP, or m-DXP, respectively (Scheme 2). High dye loadings have been realized in many cases. The maximum occupation numbers are, however, rarely reached, mainly for thermodynamic and kinetic reasons. We distinguish between one-, two-, and three-dye composites, but we do not discuss more complex patterns. Acceptors are distributed randomly inside the crystals in composite b'' (Scheme 1). Sequential insertion for synthesizing sandwich-structure composites is simple, in principle. However, finding the right loading conditions can be more difficult.<sup>[37]</sup> Perylene-3,4:9,10-tetracarboxylic



**Scheme 2.** Top: Comparison of the length of three dyes, HR (1.5 nm), DMP (2 nm), and m-DXP (2.4 nm), with the u.c. length of ZL. The two yellow vertical lines mark the 1.5 nm length of two u.c.s. Bottom: Illustration of the van der Waals surfaces of tb-DXP (2.7 nm; upper) and ADE-XP (3.1 nm; lower) with the 12-ring channel opening of ZL. Numbers in parentheses are the van der Waals lengths of the molecules (see Tables 1 and 2 for structures).

diimides (PDIs; Table 1) represent classical structure types of colorants that have attracted tremendous interest in fundamental and industrial research.<sup>[38]</sup>

Assembling these dyes in a precise multichromophore supramolecular scaffold with DNA has been investigated,<sup>[39]</sup> and has recently led to the discovery of two homochromophoric H-aggregates.<sup>[40]</sup> Insertion of PDIs into the channels of ZL in different laboratories resulted in a variety of composites with remarkable properties.<sup>[1,6,8,23,30,31]</sup> Most of our PDI-ZL experiments have been performed with DXP and tb-DXP. These dyes cannot be inserted at room temperature. Their largest van der Waals diameter is about 0.76 nm, and therefore, exceeds the 0.71 nm van der Waals diameter of the ZL channel opening.<sup>[41]</sup> Therefore, insertion is performed under vacuum conditions at about 200 °C. At this temperature, the breathing vibrational modes of the 12-ring channel entrance of ZL are fully activated<sup>[42]</sup> and the PDIs can slip through. In zeolite nomenclature, a 12-ring consists of 12T atoms (T = Si, Al) plus 12 bridging oxygen atoms.<sup>[41,42]</sup> Conditions and structural details that enhance or hinder insertion and transport in ZL channels are, however, not well understood. We therefore report a comparison between 17 differently substituted PDIs, two terylene diimides (TDIs), and a quaterylene diimide (QDI; Tables 1 and 2). PDIs are especially well suited for studying the structure-transport relationship of dyes in ZL because their core fits tightly through the 12-ring channel opening and the substituents at both ends of the dyes can be easily varied without significantly influencing their electronic absorption and fluorescence spectra. Sequential insertion of different dyes leads to sandwich structures, and hence, allows the formation of sophisticated antenna composites for light harvesting, transport, and trapping. Herein, we describe the synthesis of a rationally

**Table 1.** Insertion of PDIs into the channels of ZL. The insertion temperature was 260 °C and the zeolite host, ZL, was of barrel type, unless stated otherwise. The absorption spectra of the PDIs are very similar, with a molar extinction coefficient of about 88 200 m<sup>-1</sup> cm<sup>-1</sup> at 525 nm in CH<sub>2</sub>Cl<sub>2</sub>.

Structure	Name/loading <sup>[a]</sup> [%]	Structure	Name/loading <sup>[a]</sup> [%]
	tdc-XP/29 (40) (180 °C)		dmpa-XP/43 (67) (220 °C)
	DXP/48 (67) ZL <sub>T5</sub>		dm-DXP/57 (67)
	tb-DXP/48 (67) ZL <sub>T5</sub>		m-DXP/41 (67)
	b-DXP/17 (67)		ip-DXP/51 (67)
	(dmp)-DXP/31 (67)		
	bone-DXP/40 (80) (250 °C)		o-bone-DXP/40 (80) (250 °C)
	DEXP/19 (67)		ADE-XP/ < 2 (53)
	DIXP/ < 3 (73)		dm-XP/19 (67) (300 °C)
	tb-XP/ZL <sub>T5</sub> decomp (67)		b-XP/ZL <sub>T5</sub> decomp (67)

[a] The effective and target loadings are given as percentages, the latter in parenthesis, with respect to the theoretical maximum loading.

**Table 2.** Dyes used for the preparation of different dye–ZL composites. The solvent was CH<sub>2</sub>Cl<sub>2</sub>, unless stated otherwise. The ZL host was of barrel type.

Structure	Name/loading <sup>[a]</sup> [%]	Absorption λ [nm] (ε [dm <sup>3</sup> mol <sup>-1</sup> cm <sup>-1</sup> ])	Emission λ [nm]
	dmpa-XT/0 (280 °C)	653 (106 000) 600 (55 796) 555 (7053)	672 (exc. 620)
	tb-DXT/4.5 (7.5) (270 °C)	653 (106 000) 600 (55 796) 555 (7053)	673 (exc. 620)
	tb-DXQ/5 (17) (270 °C)	764 (155 000) 708 (72 272)	828 (exc. 690)
	HR/60 (200 °C) (0.5 IMZ <sup>+</sup> /u.c.)	527 (20 000)	566 (exc. 490)
	DMP/60 (200 °C)	363 (41 420) <sup>[b]</sup>	430 (exc. 340)

[a] Loadings, and target loadings in parentheses, are given in terms of 4.5 u.c./site for tb-DXT, 5 u.c./site for tb-DXQ, and 3 u.c./site for HR and DMP. [b] The solvent was 1-butanol.

designed library of substituted PDIs and TDIs, as well as a QDI, and correlate the substituent type with insertion behavior and

properties of the resultant composites, including two- and three-color antenna systems.

It is convenient to describe the loading of a dye–ZL composite in terms of the occupation probability or loading,  $p$ , which is defined as the ratio between the numbers of occupied sites divided by the total number of sites available. The value of  $p$  ranges from zero for an empty ZL to one for a fully loaded ZL. A site expresses the number of u.c.s occupied by a guest. The dye concentration in terms of molar volume as a function of  $p$  is expressed by Equation (1), in which  $n_s$  is the number of u.c.s that can be occupied by a guest.<sup>[1]</sup>

$$c(p) = 0.752 \frac{p}{n_s} \left( \frac{\text{mol}}{\text{L}} \right) \quad (1)$$

The numbers in the composite names, such as dye–ZL.31, indicates the dye loading  $p$ . In a sandwich composite of two dyes, we write dye1,dye2–ZL.05,.12, in which .05 refers to dye2 and .12 to dye1. The default 3.6 charge-compensating cations per u.c. of ZL, which can be replaced by means of cation exchange, are  $K^+$ . We often replace some of them by the organic cation  $IMZ^+$ .<sup>[43]</sup> The name of such composites is, for example, dye1,dye2–ZL.05,.12(0.5 $IMZ^+$ ), which means that 0.5 $K^+$  per u.c. have been replaced by  $IMZ^+$ .

## Results and Discussion

### Synthesis of dyes

The preparation of the investigated dyes can be divided into the following classes (Tables 1 and 2): 1) commercially available dyes, 2) PDIs, 3) TDIs, and 4) QDIs.

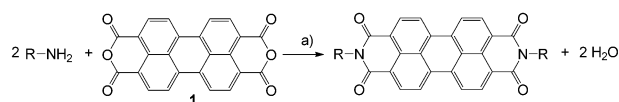
### Commercially available dyes

The following commercially available dyes were investigated herein: 2,9-bis(2,6-dimethylphenyl)anthra[2,1,9-*def*:6,5,10-*d'e'f'*]-diisoquinoline-1,3,8,10(2*H*,9*H*)tetraone (DXP), 2,9-bis(3,5-dimethylphenyl)anthra[2,1,9-*def*:6,5,10-*d'e'f'*]diisoquinoline-1,3,8,10-(2*H*,9*H*)-tetraone (Pigment Red 149, for which we have used the abbreviation dm-XP), 14*H*-anthra[2,1,9-*mna*]thioxanthen-14-one (Hostasol Red, for which we have used the abbreviation HR), and 1,4-bis(4-methyl-5-phenyloxazol-2-yl)benzene (DMP).

### PDI dyes

Most PDI dyes were prepared by applying a simple condensation reaction in which perylene-3,4,9,10-tetracarboxylic dianhydride (**1**) was treated with appropriate amines in quinoline or imidazole as solvent with zinc acetate as a catalyst at 180–240 °C for several hours under an inert atmosphere, and the yields were in the range of 7 to 95% (Scheme 3). Therefore, the main challenge was the preparation of the corresponding amines.

The PDI dyes prepared from commercially available amines were as follows (reaction conditions are given in parentheses): DXP ( $Zn(OAc)_2$ , quinoline, 230 °C, 4 h, 73%), DEXP ( $Zn(OAc)_2$ , quinoline, 220 °C, 24 h, 47%), DIXP ( $Zn(OAc)_2$ , imidazole,

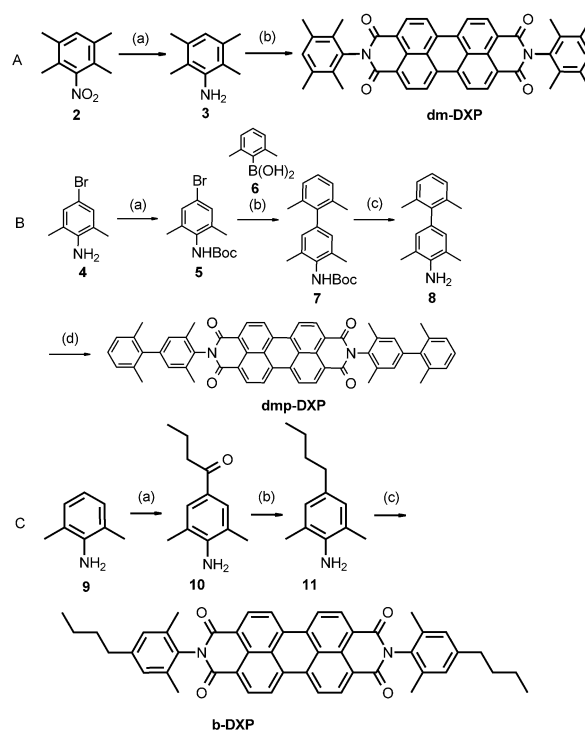


**Scheme 3.** General synthesis of PDI dyes. Reagents and conditions: a)  $Zn(OAc)_2$ , imidazole/quinoline/diethanolamine, 190–250 °C, 4–48 h, 7–95% yield.

140 °C, 24 h, 8%), tb-XP (diethanolamine, 180 °C, 6 h, 78%), m-DXP ( $Zn(OAc)_2$ , quinoline, 230 °C, 4 h, 73%), and b-XP ( $Zn(OAc)_2$ , quinoline, 230 °C, 4 h, 95%).

The following PDI dyes were prepared with amines described in literature. In parentheses are given the condition for the last step of the synthesis (dye formation). tdc-XP ( $Zn(OAc)_2$ , imidazole, 190 °C, 4 h, 73%),<sup>[44]</sup> tb-DXP ( $Zn(OAc)_2$ , quinoline, 230 °C, 4 h, 66%),<sup>[45,46]</sup> and dmpa-XP ( $Zn(OAc)_2$ , imidazole, 190 °C, 24 h, 8%).<sup>[47]</sup> The following series of reaction schemes show the preparation of PDI dyes with amines that are insufficiently or not described in the literature.

Compound **2** (Scheme 4 A) was reduced with zinc powder in combination with  $CaCl_2$  in EtOH to give **3** in 67% yield. Compound dm-DXP was then prepared in 32% yield through the condensation of **3** with **1**, by using  $Zn(OAc)_2$  in quinoline.<sup>[48]</sup> Interestingly, this was the only PDI derivative of the series that readily formed crystals ( $CH_2Cl_2$ , concentrated solution, RT).



**Scheme 4.** A) Synthesis of dm-DXP. Reagents and conditions: a) Zn,  $CaCl_2$ , EtOH, 75 °C, 16 h, 67%; b) **1**,  $Zn(OAc)_2$ , quinoline, 240 °C, 48 h, 32%. B) Synthesis of (dmp)-DXP. Reagents and conditions: a)  $Boc_2O$  (Boc = *tert*-butyloxy-carbonyl), EtOH, RT, 48 h, quant.; b)  $Pd(OAc)_2$ ,  $Ph_3P$ ,  $K_2CO_3$ , THF/ $H_2O$  (2:1), 80 °C, 24 h, 91%; c) 4 M HCl/dioxane,  $H_2O$ , 90 °C, 1 h, 32%; d) **1**,  $Zn(OAc)_2$ , quinoline, 240 °C, 48 h, 13%. C) Synthesis of b-DXP. Reagents and conditions: a) Butyric acid, polyphosphoric acid (PPA), 175 °C, 3.5 h, 33%; b)  $Et_3SiH$ ,  $CF_3CO_2H$ , RT, 2 h, 85%; c) **1**,  $Zn(OAc)_2$ , quinoline, 240 °C, 48 h, 19%.

The amino group of 4-bromo-2,6-dimethylaniline (**4**) was protected with Boc (Scheme 4B) by using  $\text{Boc}_2\text{O}$  in EtOH to give **5** quantitatively. The latter was used in a Suzuki coupling protocol with 2,6-dimethylphenylboronic acid (**6**) to produce biphenyl derivative **7** in 91 % yield. Standard Boc removal conditions (trifluoroacetic acid (TFA) in  $\text{CH}_2\text{Cl}_2$ ) proved inefficient, so compound **7** was deprotected by using 4 M HCl in dioxane at  $90^\circ\text{C}$  to give **8** in 32 % yield. Compound (dmp)-DXP was then prepared in 13 % yield through the condensation of **8** with **1** by using  $\text{Zn}(\text{OAc})_2$  in quinoline. Compound **9** was acylated with butyric acid in PPA (Scheme 4C), which produced **10** in 33 % yield. The latter was reduced with triethylsilane in TFA to give **11** in 85 % yield. Compound b-DXP was then prepared in 19 % yield through the condensation of **11** with **1**, by using  $\text{Zn}(\text{OAc})_2$  in quinoline.

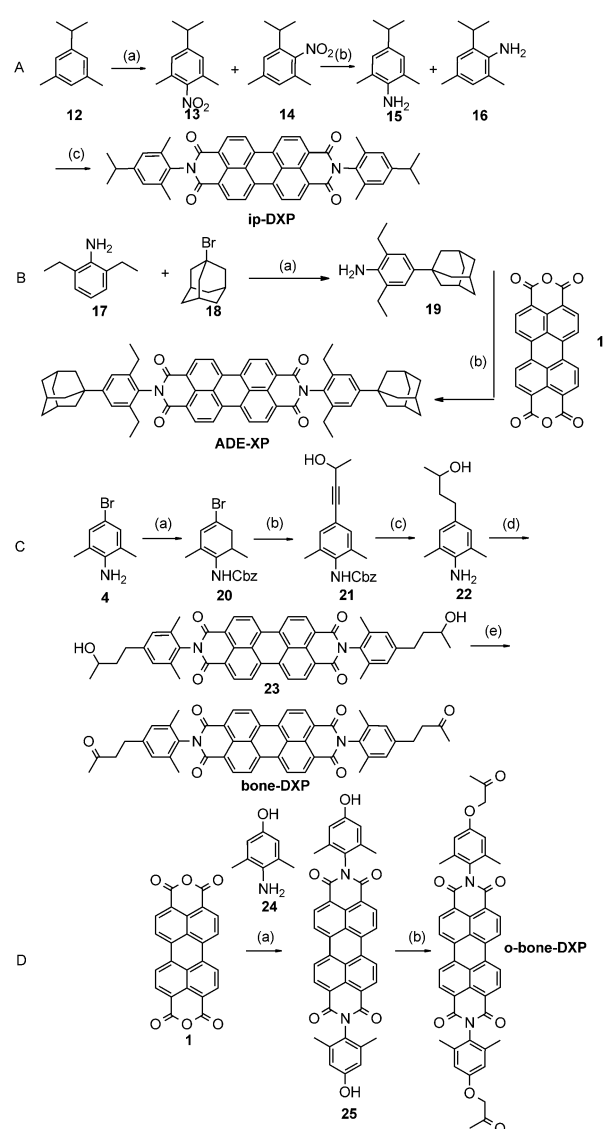
Compound **12** (Scheme 5A) was nitrated by using a combination of fuming nitric acid/acetic anhydride in acetic acid to yield a mixture of regioisomers **13** and **14** in 71 % yield. The  $R_f$  values of the regioisomers were too similar for separation by flash chromatography; therefore, the mixture was reduced with zinc powder in ethanol. The resultant aniline derivatives **15** and **16** give, after purification, compound **15** in 12 % yield. Compound ip-DXP was then prepared in 7 % yield through the condensation of **15** with **1**, by using  $\text{Zn}(\text{OAc})_2$  in quinoline. Compound ADE-XP (Scheme 5B) was prepared by the condensation of **17** with **18** at  $200^\circ\text{C}$  for 4 h to give **19** in 48 % yield. Subsequent condensation of **19** with **1** by using zinc acetate as a catalyst in quinoline at  $220^\circ\text{C}$  gave ADE-XP in 13 % yield.

The amino group of **4** was protected with Cbz (Scheme 5C) by using  $\text{CbzCl}$  and  $\text{NaHCO}_3$  in THF to give **20**. The coupling of **20** and 3-butyne-2-ol with  $[\text{Pd}(\text{PPh}_3)_2\text{Cl}_2]$  and  $\text{CuI}$  in THF/ $\text{Et}_3\text{N}$  gave **21** in 15 % yield. The Cbz protecting group of **21** was cleaved and the triple bond was fully reduced simultaneously with  $\text{H}_2$  and Pd/C in MeOH to give **22** in 76 % yield. Compound **22** was then condensed with **1** by using  $\text{Zn}(\text{OAc})_2$  in quinoline to give **23** in 12 % yield. The diol was then oxidized to give diketone bone-DXP in 25 % yield by using PCC in  $\text{CH}_2\text{Cl}_2$ . Compound *o*-bone-DXP (Scheme 5D) was prepared through the condensation of 4-amino-3,5-dimethylphenol (**24**) with **1** by using  $\text{Zn}(\text{OAc})_2$  in quinoline to give **25** in 60 % yield. Subsequent alkylation with chloroacetone by using  $\text{K}_2\text{CO}_3$  and KI in DMF gave *o*-bone-DXP in 57 % yield. The synthetic procedures for tdc-XP, dmpa-XP, b-XP, tb-XP, m-DXP, tb-DXP, DIXP, and DEXP are described in the Supporting Information.

### TDI dyes

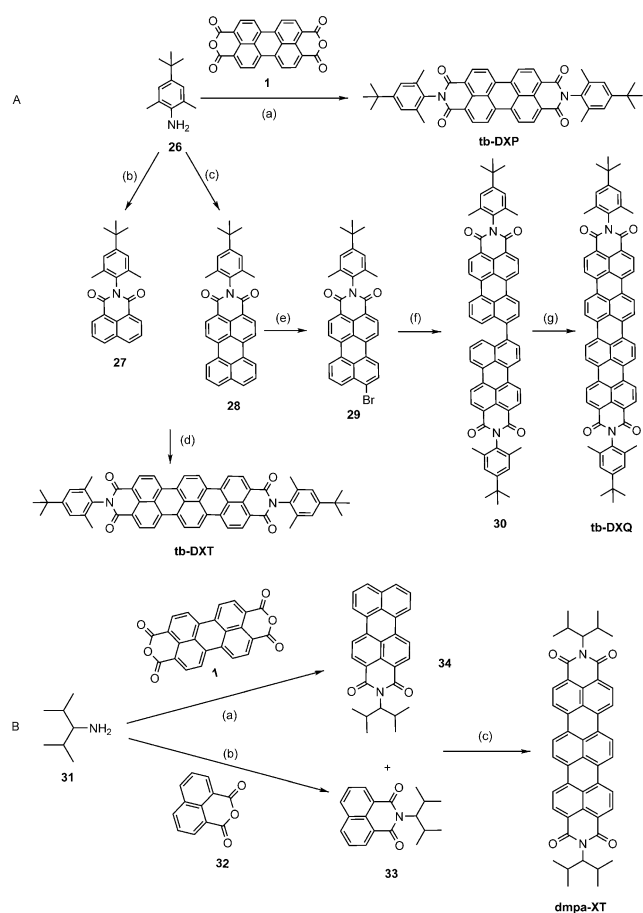
The TDI dyes are more challenging to synthesize.<sup>[49]</sup> An appropriate dianhydride precursor, such as **1** for the preparation of PDI dyes, is missing. Therefore, a step-by-step procedure to construct the TDI core was the strategy used to obtain the desired dyes, tb-DXT and dmpa-XT.

The aniline derivative (**26**; Scheme 6A)<sup>[45,46]</sup> was condensed with **1** by using  $\text{Zn}(\text{OAc})_2$  in quinoline at  $230^\circ\text{C}$  for 4 h to give tb-DXP in 66 % yield. For the synthesis of the TDI derivative tb-DXT, first, 1,8-naphthalic anhydride (**32**) was condensed with **26** in acetic acid at reflux to give **27** in 56 % yield. Then com-



**Scheme 5.** A) Synthesis of ip-DXP. Reagents and conditions: a) fuming  $\text{HNO}_3$ ,  $\text{Ac}_2\text{O}$ , acetic acid, RT, 2 h, 71 %; b) Zn,  $\text{CaCl}_2$ , EtOH,  $75^\circ\text{C}$ , 16 h, 12 %; c) **1**,  $\text{Zn}(\text{OAc})_2$ , quinoline,  $240^\circ\text{C}$ , 48 h, 7 %. B) Synthesis of ADE-XP. Reagents and conditions: a) 2,6-diethylaniline (**17**; commercially available), 1-bromoadamantane (**18**; commercially available),  $200^\circ\text{C}$ , 4 h; b) **1**,  $\text{Zn}(\text{OAc})_2$ , quinoline,  $220^\circ\text{C}$ , 24 h, 13 %. C) Synthesis of bone-DXP. Reagents and conditions: a) benzyl chloroformate (CbzCl),  $\text{NaHCO}_3$ , THF, RT, 8 h, 78 %; b) 3-butyne-2-ol,  $[\text{Pd}(\text{PPh}_3)_2\text{Cl}_2]$ ,  $\text{CuI}$ , THF/ $\text{Et}_3\text{N}$ ,  $55^\circ\text{C}$ , 2 d, 15 %; c)  $\text{H}_2$ , Pd/C, MeOH, RT, 2 d, 76 %; d) **1**,  $\text{Zn}(\text{OAc})_2$ , imidazole,  $240^\circ\text{C}$ , 48 h, 12 %; e) pyridinium chlorochromate (PCC),  $\text{CH}_2\text{Cl}_2$ , RT, 5 h, 25 %. D) Synthesis of *o*-bone-DXP. Reagents and conditions: a)  $\text{Zn}(\text{OAc})_2$ , quinoline,  $250^\circ\text{C}$ , 48 h, 60 %; b) chloroacetone,  $\text{K}_2\text{CO}_3$ , KI, DMF,  $80^\circ\text{C}$ , 12 h, 57 %.

ound **26** was reacted with **1** in the presence of water,  $\text{Zn}(\text{OAc})_2 \cdot 2\text{H}_2\text{O}$ , and imidazole, leading to partial decarboxylation–condensation to yield the monoimide derivative **28**. The latter was then fused with **27** by using  $t\text{BuONa/DBN}$  in diglyme<sup>[49]</sup> to give tb-DXT in 20 % yield. Compounds **31** and **32** were coupled at  $150^\circ\text{C}$  to give **33** in 80 % yield. In a similar reaction, under catalytic conditions in an imidazole/water mixture at  $190^\circ\text{C}$  for 24 h, compounds **1** and **31** coupled to give **34** in 52 % yield. Final coupling between **33** and **34** in toluene with  $\text{DBN}/t\text{BuONa}$  at  $130^\circ\text{C}$  for 3 h gave dmpa-XT in 8 % yield.



**Scheme 6.** A) Synthesis of tb-DXP, tb-DXT, and tb-DXQ. Reagents and conditions: a)  $\text{Zn}(\text{OAc})_2$ , quinoline, 240 °C, 48 h, 56%; b) **32**,  $\text{CH}_3\text{CO}_2\text{H}$ , reflux, 24 h, 56%; c) **1**,  $\text{Zn}(\text{OAc})_2 \cdot 2\text{H}_2\text{O}$ ,  $\text{H}_2\text{O}$ , imidazole, 245 °C, 4 d, 88%; d)  $t\text{BuONa}$ , 1,5-diazabicyclo[4.3.0]non-5-ene (DBN), diglyme, 155 °C, 24 h, 20%; e)  $\text{Br}_2$ , chlorobenzene, 50 °C, 4 h, quant.; f)  $[\text{Ni}(\text{cod})_2]$ , 2,2'-bipyridine (bipy), 1,5-cyclooctadiene (cod), DMF, 70 °C, 48 h, 53%; g)  $\text{KOH}$ ,  $\text{D-glucose}$ , EtOH, 120 °C, 3 h, 85%. B) Synthesis of dmpa-XT. Reagents and conditions: a) **1**, **31**,  $\text{Zn}(\text{OAc})_2$ , imidazole/ $\text{H}_2\text{O}$ , 190 °C, 24 h, 52%; b) **31**, **32**,  $\text{Zn}(\text{OAc})_2$ , imidazole, 150 °C, 4.5 h, 80% for **33**; c) **33**, **34** in dry toluene,  $t\text{BuONa}$ , DBN, 130 °C, 3 h, 8%.

### QDI dye

The QDI derivative (tb-DXQ) was prepared by using a method developed by Müllen et al. (Scheme 6A).<sup>[50,51]</sup> Bromination of **28** gave compound **29** and subsequent Yamamoto homocoupling<sup>[52]</sup> with  $[\text{Ni}(\text{cod})_2]$  and bipy gave biaryl **30**, which was then cyclized to give tb-DXQ with  $\text{KOH}$ <sup>[53]</sup> in 85% yield.

### Insertion of dyes into the ZL nanochannels

Neutral dyes are inserted into the channels of ZL by dissolving them in a volatile solvent, usually  $\text{CH}_2\text{Cl}_2$ , and then soaking the crystals in this solution. The sample is dried under vacuum to remove the solvent and water. The dyes adsorb on the ZL crystal surfaces during this process. The evacuated glass container is sealed and kept for the required time (hours to days) at a temperature at which the dyes become sufficiently mobile. The temperature regime applied to the PDIs ranges from 180 to 300 °C, depending on their mobility and thermal stability.

The 17 dyes we have investigated fall into 4 categories. In the first, we have two examples (tdc-XP and dmpa-XP; Table 1) with aliphatic groups attached to nitrogen. Both can be inserted at 180 and 220 °C, but decompose at higher temperatures. We distinguish between the target loading, which refers to the composition of the reaction mixture, and the effective loading, which refers to the final product. The fact that tdc-XP enters the zeolite better than one might expect can be explained by assuming that the aliphatic C7 tails coil in a manner that allows them to slip through the narrow channel opening. The most important class consists of 9 dyes with methyl groups at the 2- and 6-positions of the imide phenyl groups, which prevent strong  $\pi$ -stacking. All 9 of them can be inserted at 260 °C with an effective to target loading ratio higher than 0.6, with the exception of b-DXP and (dmp)-DXP, which enter more reluctantly. The 2 dyes with carbonyl groups at both ends (bone-DXP and *o*-bone-DXP) enter more easily and are therefore inserted at 250 °C. The use of ethyl at the 2- and 6-positions instead of methyl still allows the DEXP to enter, but it seems that the molecule becomes too stiff if adamantyl is added, so that ADE-XP cannot be inserted in a significant amount. It is less surprising that DIXP, with isopropyl at the 2- and 6-positions, cannot be inserted. The final category consists of PDIs without substituents at these positions, namely, tb-XP, b-XP, and dm-XP. These dyes lack the 2- and 6 methyl groups, and therefore, form stable aggregates as a result of strong  $\pi$ -stacking. Only dm-XP can be inserted to a significant amount. However, a higher temperature is needed, which it appears to tolerate under the applied vacuum conditions. The other two dyes decompose at 260 °C either at the surface or inside of the host. We investigated the ratio of effective loading to target loading for values of 2, 40, 60, and 80% for *o*-bone-DXP at 250 °C. The result was always 0.5. This means that we do not reach the saturation region and a higher loading is possible if Langmuir behavior is assumed, which is reasonable. This behavior has been observed for the insertion of cationic dyes through cation exchange.<sup>[1]</sup> If we correlate the ratio of effective loading against target loading (each 50%) in the series dm-DXP, ip-DXP, tb-DXP, m-DXP, and b-DXP, we find values of 0.86, 0.76, 0.72, 0.62, and 0.26. This leaves us with the impression that the aliphatic character of the substituted phenyl ring is crucial for the movement of dyes on the external ZL surface and in the channels. Butyl-substituted b-DXP does not seem to follow this line for reasons we do not yet understand. To further investigate the structure to loading behavior, we tested two TDIs and one QDI. We found that tb-DXT could be inserted at 270 °C with an effective loading to target loading ratio of 0.6. The value for tb-DXQ was 0.3, whereas dmpa-XT could not be inserted (Table 2). This means that 1) the *tert*-butyl (tb)-tail supports transport within the channels, 2) aliphatic groups directly attached to nitrogen are less favorable, and 3) the length of the molecules is less critical than one might expect. To better understand the loadings of tb-DXT and tb-DXQ, it is useful to realize that they correspond to 6 or 7 molecules per channel and approximately 440 000 dye molecules per ZL crystal. Synthesizing ZL may sometimes be an obstacle for using this versatile material as a host. We have therefore not only

tested ZL, but also the commercially available product ZL<sub>75</sub>. The latter was found to be useful for basic test experiments. If purity, morphology, size, and size distribution are important, then it is advantageous to use ZL crystals prepared according to one of several published methods.<sup>[18–23]</sup> Apart from a relatively small bathochromic shift, it is a general observation that the shape of the absorption and fluorescence spectra of molecules inside the ZL channels changes little compared with the shape in solution. In many cases, the vibrational structure seen in solution is well preserved in the dye–ZL composites, whereas in other examples some broadening is seen.<sup>[1,54]</sup> Larger spectral changes are often caused by saturation effects, self-absorption of highly loaded samples,<sup>[23]</sup> and J-aggregate coupling.<sup>[31–34]</sup> The spectra of DMP, tb-DXP, and HR shown in Figure 1 fit well into this general pattern. Although some broadening and red-shifting is seen in the spectra of DMP–ZL and HR–ZL, the shift and broadening of the tb-DXP–ZL spectrum is small and the vibrational structure is preserved.

These three dyes were chosen for the construction of a three-dye antenna cascade because they showed perfect spectral overlap (Table 3), which is a requirement for a good antenna. Their length and shape is such that they align inside the ZL channel with their S<sub>0</sub>–S<sub>1</sub> electronic transition moment parallel to the channel axis, which is the best possible situation for efficient FRET.<sup>[36,55]</sup>

This was tested by inserting the dyes into ZL crystals of about 5 μm in length, which allowed the optical dichroism to be measured by means of fluorescence microscopy. The results of such measurements (Figure 2) demonstrate the anisotropy.

Donor/Acceptor	$J_v$ [cm <sup>3</sup> M <sup>-1</sup> ]	$R_0$ [nm] ( $\kappa^2 = 4$ )	$R_0$ [nm] ( $\kappa^2 = 1$ )
DMP (homo)	$5.4 \times 10^{-15}$	4.1	3.2
DMP/tb-DXP	$1.15 \times 10^{-13}$	6.8	5.4
DMP/HR	$4.53 \times 10^{-14}$	5.8	4.6
tb-DXP (homo)	$2.03 \times 10^{-13}$	7.4	5.9
tb-DXP/HR	$1.37 \times 10^{-13}$	7.0	5.6
HR (homo)	$3.82 \times 10^{-14}$	5.6	4.4

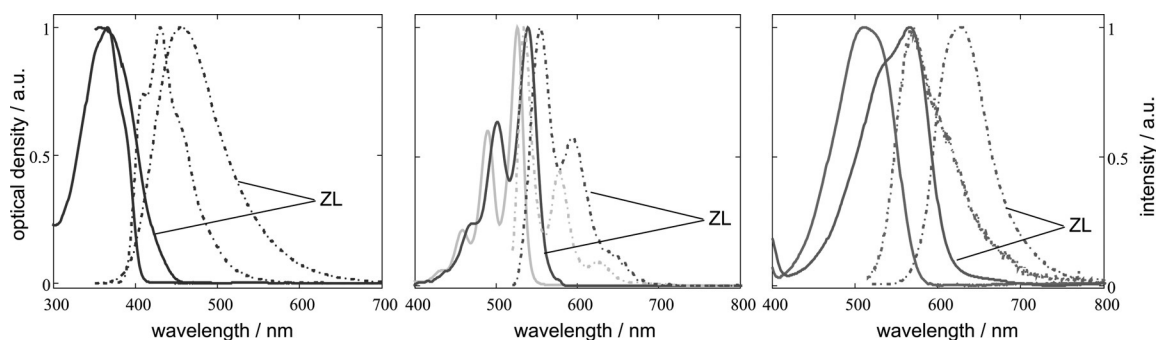


Figure 1. Absorption (—) and fluorescence (---) spectra of dyes in solution and those of dye–ZL composites. Left: DMP (1-butanol) and DMP–ZL.2. Middle: tb-DXP (CH<sub>2</sub>Cl<sub>2</sub>) and tb-DXP–ZL.002 (dark grey). Right: HR (CH<sub>2</sub>Cl<sub>2</sub>) and HR–ZL.1. The spectra of the dye–ZL composites were measured as oil–glass sandwich (OGS)<sup>[23]</sup> layers and are indicated as ZL.

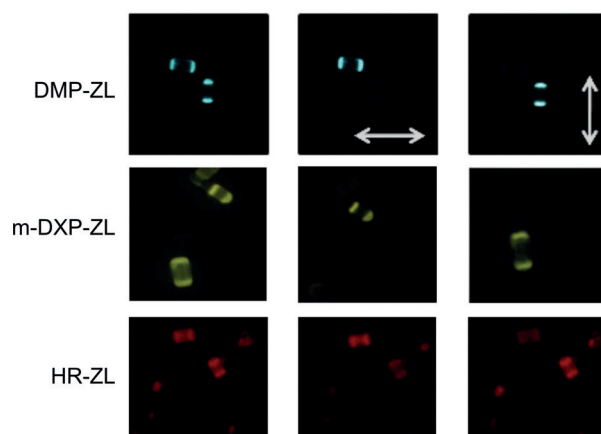
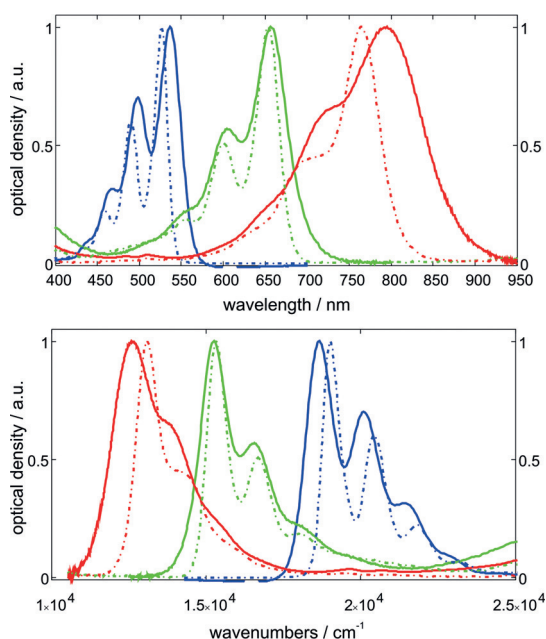


Figure 2. Optical fluorescence microscopy images of 5 μm long ZL crystals partially loaded with dyes: top: DMP–ZL, middle: m-DXP–ZL, bottom: HR–ZL. The images on the left were observed without a polarizer; the middle row when applying a horizontally oriented polarizer, as indicated by the double arrow; and in the right row the polarizer was oriented perpendicularly.

The same result as that shown for m-DXP–ZL was observed for DXP–ZL, dm-XP–ZL, and tdc-XP–ZL. Thus, we can safely assume that it applies to all PDI–ZL composites reported in Table 1. The crystals were only partially loaded, so that the dyes did not have time to diffuse into the middle part of the long crystals. We therefore see high intensity at both ends of the crystals and a dark part in the middle.

The absorption and fluorescence spectra of all PDIs in degassed CH<sub>2</sub>Cl<sub>2</sub> and those of the PDI–ZL composites change very little, and the measured extinction coefficients are very similar. Moreover, all show high fluorescence quantum yields in solution and as dye–ZL composites, with the exception of *o*-bone-DXP, which has a quantum yield about 10 times lower in solution and in ZL. This matches observations by Langhals et al.,<sup>[56]</sup> who reported that a similar *para*-methoxy-substituted dye showed a much lower quantum yield than that of DXP.<sup>[23]</sup>

In Figure 3, the absorption spectra of tb-DXP–ZL, tb-DXT–ZL, and tb-DXQ–ZL are compared. The spectra in wavelengths (Figure 3, top) give the impression that spectral changes are larger for tb-DXT and tb-DXQ than those for tb-DXP. This



**Figure 3.** Absorption spectra of tb-DXP (blue), tb-DXT (green), and tb-DXQ (red) as  $5 \times 10^{-6}$  M solutions (---) in  $\text{CH}_2\text{Cl}_2$  and as dye-ZL composites (—), given in wavelenghts (top) and wavenumbers (bottom).

wrong impression is corrected when plotting the spectra in wavenumber (Figure 3, bottom). The characteristic vibronic structure of PDI dyes, also present in TDI and QDI dyes, has been used to analyze their interaction with the inner surface of the ZL nanochannels by comparing the positions of the 0–0', 0–1', 0–2', and 0–3' transitions, which can be identified in dilute solutions of these dyes. This allows us to draw the conclusion that the energy difference,  $\Delta E[\nu' - (\nu' + 1)]$ , between the 0– $\nu'$  and 0–( $\nu' + 1$ ) transitions is the same in solution and in ZL. These observations can be interpreted in terms of a weak interaction of the chromophoric core of these dyes with the inner surface of the ZL nanochannels (for details, see the Supporting Information). We have observed, however, that the cocations exert a stronger influence on the fluorescence spectra of tb-DXT and tb-DXQ than that seen for the PDIs; this demands a dedicated investigation.

### Stopcock and surface modification

The surface hydroxyl groups of zeolites can be used for the modification and fine-tuning of the particle properties. The grafting of silane coupling agents with trialkoxysilyl or trichlorosilyl groups to zeolites and mesoporous materials has been investigated extensively.<sup>[13,25,57–60]</sup> As a consequence of the hexagonal structure of ZL crystals, which can be approximated by cylinders, the coat and base surfaces have different reactivity. It is therefore possible to selectively modify them. Selective modification has been used to organize zeolite microcrystals into 2D functional entities, such as monolayers, multilayers, and patterned monolayers, on various substrates.<sup>[24–28]</sup> It has also been used to selectively modify the base that bears the

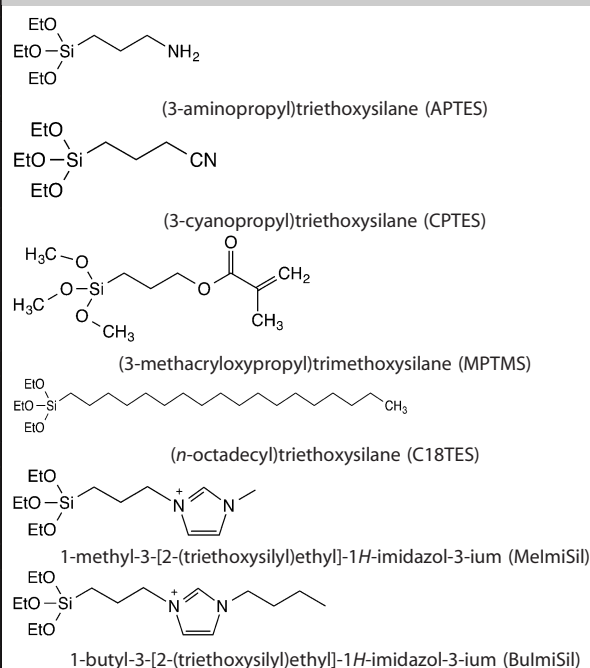
channel entrances to customize its properties or just for sealing, preventing guests from leaving the channels.<sup>[1,5,60,61]</sup>

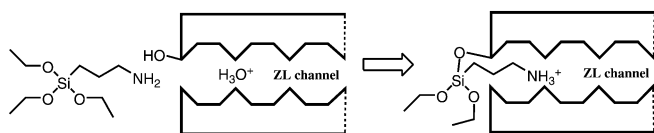
Sealing the channels for molecules such as DXP, rare-earth complexes, or HR was achieved by adsorbing branched polyethyleneimine (PEI) on the ZL surface.<sup>[30,62,63]</sup> This procedure is, however, less specific than modification with trialkoxysilyl and fine-tuning is not supported. It also has the effect of increasing the size of the particles substantially because it cannot be applied selectively on the base and also because multilayer coating is necessary. It was found to hinder dispersibility in organic matrices.

We have observed that the grafting of trialkoxysilanes onto ZLs, either in a stopcock manner on the base or for surface modification on the coat, leads to superior properties and makes them more versatile for handling as functional composite particles. Modification of ZL surfaces with trialkoxysilyl agents has been used to synthesize oriented monolayers of zeolite crystals on different substrates.<sup>[24–28]</sup> We have therefore tested the molecules collected in Table 4 for surface modification. The stopcock modification reaction is explained for APTES in Scheme 7. APTES adsorbs specifically at the basal surface of the ZL crystals at the acidic<sup>[1,30]</sup> channel entrances, which encourages protonation of the amine, and hence, its entering more deeply into the channel. It then binds covalently through condensation with an OH group at the surface. It remains difficult to experimentally determine details and the number of covalent siloxane bonds that fix the stopcock head to the channel entrance.

Based on extensive theoretical studies, we know that Al–OH groups at the entrances are the preferred modification sites and that bipodally modified entrances are possible, but may suffer from strain, whereas tripod modifications can be ruled out.<sup>[64]</sup>

**Table 4.** Molecules for stopcock and surface modification.





**Scheme 7.** Insertion of APTES and the formation of covalent bonds with silanol groups at the ZL channel entrances.

The results of leaking tests performed with ZL crystals loaded with HR are shown in Figure 4. The samples were stored in transparent glass bottles, at RT, on the laboratory bench. HR was chosen for these experiments because it leaked out much faster than tb-DXP in uncoated samples, so test results obtained with HR-ZL samples were more conclusive. The procedure used for plugging the channels had no influence on the absorption and fluorescence spectra of the composites. The unsealed HR-ZL sample showed significant leakage after

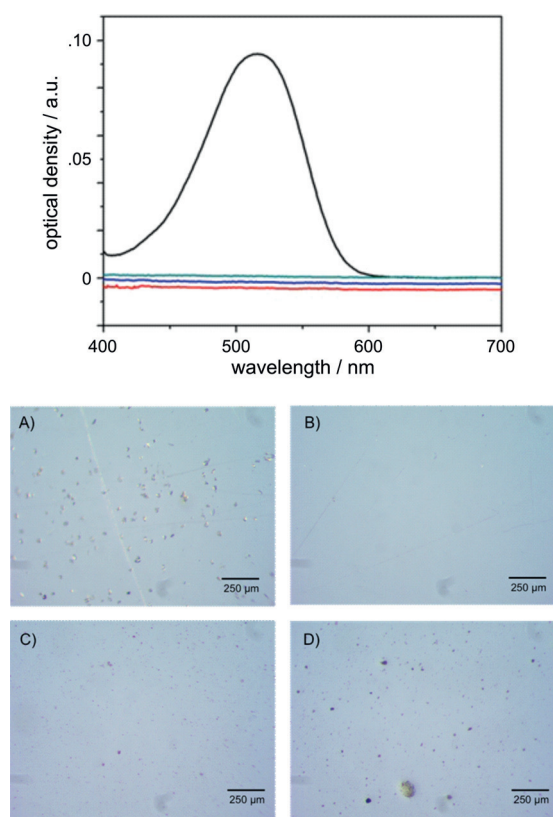


**Figure 4.** Top: Results from leaking tests. UV/Vis absorption spectra of the filtered washing solution of open and stopcock-plugged HR-ZL samples tested after one month of storage: HR-ZL<sub>TS</sub>-20(0.75 IMZ<sup>+</sup>) (black), HR-ZL<sub>TS</sub>-20(0.75 IMZ<sup>+</sup>)@BulmiSil (red), HR-ZL<sub>TS</sub>-20(0.75 IMZ<sup>+</sup>)@MelmiSil (blue), and HR-ZL<sub>TS</sub>-20(0.75 IMZ<sup>+</sup>)@APTES (green). The blue and red spectra have been displaced to better show their shape. Bottom: Microscopy images of thin poly(methyl methacrylate) (PMMA) films with and without dye-ZL. All films were cast from solutions of PMMA in toluene at a concentration of 100 mg mL<sup>-1</sup> PMMA. A) Pure PMMA film cast without preliminary filtration. B) Cast from a PMMA solution that was filtered through a 0.22 μm syringe filter. C) HR-ZL<sub>TS</sub>-16(0.5 IMZ<sup>+</sup>)@APTES/PMMA film cast from a filtered solution of PMMA. D) Film cast from the same material as that used in C), but without prior filtration.

one month, whereas absolutely no leakage was observed for the stopcock-plugged samples. We know, however, that APTES permits the entry of small molecules, such as water, acetonitrile and methanol. Therefore, more complete sealing is also achieved for small molecules by using the imidazolium-based stopcock molecules MelmiSil and BulmiSil (Table 4).

### Embedding dye-ZL composites into matrices and photochemical stability

The embedding of ZL particles into a polymer matrix to obtain transparent layers can be difficult, mainly because of their tendency to agglomerate; therefore, specific embedding methods have been reported.<sup>[65]</sup>

Dye-ZL composites sealed with APTES are much easier to disperse in PMMA films than unsealed ones. Composites without APTES modification show a greater tendency to form agglomerates under similar conditions. Upon examining optical microscopy images of such films, we have observed that a solution of PMMA in toluene or acetonitrile would often contain a rather large amount of undissolved material (Figure 4A). These PMMA particles are problematic because they act as agglomeration nuclei for the composites (Figure 4D). However, once the solution of PMMA is filtered, the cast film is free of such polymer blocks, and the dye-ZL crystals agglomerate much less than in the previous case (see Figure 4B and C, respectively). Both films have a dye-ZL concentration of 1 mg per 100 mg of PMMA. Good dispersion of the primary particles is of great importance for optical applications, since larger agglomerates will lead to increased light scattering of the dye-ZL/PMMA suspension. The APTES-modified dye-ZL composites, which were further functionalized by grafting MPTMS, CPTES, and C18TES (Table 4), showed good dispersibility in nonpolar organic solvents and in PMMA. C18TES-modified samples showed the best behavior in these experiments.

The stability of the transparent dye-ZL PMMA matrices under irradiation is important. We report a comparison of 100 μm thick films on a glass substrate containing dissolved tb-DXP and dispersed tb-DXP,HR-ZL<sub>TS</sub> exposed in an accelerated light stability simulator at 35 °C by using a 380 nm cutoff filter. The data in Figure 5 illustrate remarkable stabilization of the composite. The initial optical densities of the tb-DXP and tb-DXP,HR-ZL<sub>TS</sub> PMMA layers were 0.6 and 0.5, respectively. No significant changes to the shape of the absorption spectra were seen in either case. Composites modified with APTES show the same behavior as the unmodified samples. The decay is always faster at the beginning and then levels off. A similar observation was made for HR-ZL<sub>TS</sub> composites and other samples. This indicates that reactive species are present at the beginning, but are gradually used up. The decay rate slows as a consequence and perhaps becomes controlled by transport kinetics. This is supported by the observation that layers of larger optical density are photochemically more stable. It is therefore necessary to compare samples of similar optical density.

The decomposition mechanism is not well understood despite efforts to understand the photochemical degradation of

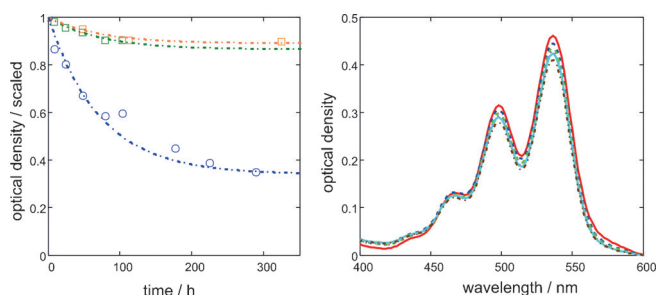


**Figure 5.** Photochemical stability upon exposure in an accelerated light stability simulator at 35 °C. Left: Optical density measured at  $\lambda = 536$  nm, scaled to 1 at 0 h irradiation time. Orange and green rectangles: two sets of experimental data for tb-DXP,HR-ZL<sub>75</sub>,04,27(0.5IMZ<sup>+</sup>) embedded in PMMA; blue circles: tb-DXP dissolved in PMMA; - - -: calculated data. Right: Absorption spectra measured after 0 (red solid line), 8, 24, 48, 79, and 103 h of exposure of tb-DXP,HR-ZL<sub>75</sub>,04,27(0.5IMZ<sup>+</sup>) embedded in PMMA.

remarkably stable Lumogen perylene dyes embedded in PMMA.<sup>[66,67]</sup> Foreign molecules present in PMMA, including oxygen and traces of solvents used to prepare the layers, may play a role. As mentioned before, APTES modification prevents leakage of dyes embedded in ZL, but does not prevent small molecules from entering the channels. Modification with stop-cocks containing a larger tail is needed to fully seal the channels.

In Figure 6 a photograph of a 100  $\mu\text{m}$  layer of tb-DXP,HR-ZL embedded in PMMA on a glass substrate is shown under illumination from the top. The PMMA/ZL layer was deposited by using a film applicator. A 1:1 solution of 1-butanol/acetonitrile



**Figure 6.** Photograph of a thin PMMA film (100  $\mu\text{m}$ ) doped with tb-DXP,HR-ZL<sub>04</sub>,25(0.5IMZ<sup>+</sup>) on a glass substrate under UV illumination.

containing 20 wt% PMMA and 1 wt% of the composite was used to apply the film. The image in Figure 6 illustrates the wave-guiding properties of the device: the edges can be clearly seen to glow orange. Such effects of the layer are of great interest for applications as, for example, luminescent solar concentrators (LSCs). An LSC is a wave-guiding plate containing luminescent chromophores. Light that falls on the face of the plate is absorbed and subsequently re-emitted at longer wavelength. The emitted light is trapped by total internal reflection and guided to the edges of the plate, where it can be, for example, collected and converted into electricity by a photovoltaic cell.<sup>[68,69]</sup>

It has been well understood for many years that a major energy loss in such a device is caused by the overlap between the absorption and emission spectra of the chromophores.<sup>[69]</sup> One way to minimize this loss is to use antenna materials, such as those described herein. Absorption and emission spectra are separated by employing a large amount of the absorbing dye and a very small amount of an emitting dye.

## Different organizational patterns of dye-ZL composites

The combinations b, b', and c shown in Scheme 1 were synthesized by using sequential procedure A. This can, in principle, lead to antenna composites for light harvesting and transport<sup>[1,23,30]</sup> that differ in the photophysical properties. System b'' can only be synthesized if a temperature regime exists for which both dyes can be inserted simultaneously, so that a random distribution of the small number of acceptors results. This has so far only been realized for cationic dyes of equal size and shape that can be inserted by ion exchange from aqueous solution.<sup>[34]</sup> The syntheses of b and b' can also differ because the dyes discussed herein have to be inserted at elevated temperatures and it is important that the dye inserted first survives the temperature regime needed for the insertion of the next one.

Furthermore, dye A experiences a different environment in the composite A<sub>2</sub>D-ZL than that in D<sub>2</sub>A-ZL because in the latter it is embedded in the environment of D. Not all dyes are sensitive to this, but HR is and has therefore been used to demonstrate this difference. The results for the three combinations (b, b', and b'') with tb-DXP as the donor and HR as the acceptor are shown in Figure 7. The absorption spectra have the same shape, with the exception of the tail at  $\lambda \approx 580$  nm.

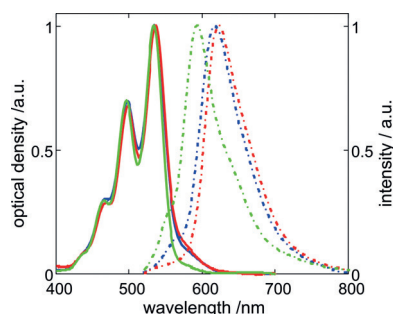


**Figure 7.** Comparison of the absorption (—) and fluorescence (---, excited at  $\lambda = 490$  nm) spectra for composites of type b, b', and b'' (Scheme 1) with tb-DXP as the donor and HR as the acceptor: tb-DXP,HR-ZL<sub>01</sub>,23(0.5IMZ<sup>+</sup>) (green), HR,tb-DXP-ZL<sub>15</sub>,04(0.5IMZ<sup>+</sup>) (red), and (tb-DXP,HR)ZL<sub>(14,05)</sub>(0.5IMZ<sup>+</sup>) (blue).

The intensity of the tail depends on the relative amount of HR with respect to tb-DXP, which is similar for the (tb-DXP,HR)-ZL<sub>(14,05)</sub>(0.5IMZ<sup>+</sup>) and HR,tb-DXP-ZL<sub>15</sub>,04(0.5IMZ<sup>+</sup>) samples, but lower for tb-DXP,HR-ZL<sub>01</sub>,23(0.5IMZ<sup>+</sup>). The tb-DXP emission is only seen as a short-wavelength tail, whereas the intense band stems from the acceptor HR. The main difference is in the fluorescence maxima. The maximum of tb-DXP,HR-ZL<sub>01</sub>,23(0.5IMZ<sup>+</sup>) in which HR is embedded between tb-DXP molecules, and therefore, essentially feels the environment of the tb tails appears at the same position as observed in CH<sub>2</sub>Cl<sub>2</sub>.<sup>[30]</sup> The largest redshift is seen in the HR,tb-DXP-ZL<sub>15</sub>,04(0.5IMZ<sup>+</sup>) sample, in which HR is located at both ends of the ZL channels, and is therefore not protected by the tb tails. The fluorescence quantum yield of tb-DXP,HR-ZL<sub>01</sub>,23(0.5IMZ<sup>+</sup>) is very good, in the order of 90%, and the

FRET efficiency of this sample has been determined to be 82% (for details, see the Supporting Information). The fluorescence quantum yield of the other two samples is lower: in the order of 50%. The fluorescence quantum yield depends on the preparation technique and on the properties of the ZL host. We assume that optimization is also possible to obtain samples with large quantum yields in these two cases. At present, we focus, however, on composites with HR in the middle. Composites of type b' with very high energy transfer and fluorescence quantum yield have been prepared with the cationic dyes oxanine and oxazine 1 as acceptor dyes (see Figure 9 of ref. [23]), for which it is more difficult to realize arrangement b (PDIs as donors) because the dyes may decompose at the temperature needed to insert the PDIs. In general, it seems to be advantageous to use neutral dyes if robust materials of high thermal and photochemical stabilities are envisaged.

### Light-harvesting antenna system

The parallel orientation of the electronic transition dipole moments of DMP, tb-DXP, and HR (Figure 2), with respect to the channels of ZL, consequently has the largest possible Förster radii ( $R_0$ ) for FRET because the orientation parameter ( $\kappa^2$ ) in Equation 2 has a maximum value of four. The spectral overlaps ( $J_v$ ) and Förster radii ( $R_0$ ) are given in Table 3. Equation 2 has been used to calculate  $R_0$ .<sup>[36,55]</sup> In this case,  $TF$  is equal to  $8.785 \times 10^{-25}$  mol, the refractive index ( $n$ ) equals 1.43, and the fluorescence quantum yield ( $\phi_{D^*}$ ) of the donor in the absence

of FRET was set to equal 1 to show the maximum  $R_0$  possible for the system. The value of  $R_0$  is only moderately influenced by small changes in  $\phi_{D^*}$ . Using Equation (3), we find, for example, that  $R_0$  decreases by about 10% if  $\phi_{D^*}$  drops by a factor of 2.

$$R_0 = \left( TF \frac{\kappa^2}{n^4} \phi_{D^*} J_v \right)^{1/6} \quad (2)$$

$$R_0(\phi_{D^*}) = R_0(1) \times \phi_{D^*}^{1/6} \quad (3)$$

The large spectral overlap of the DMP/tb-DXP, tb-DXP/HR, and tb-DXP (homo) systems, in combination with a large value for  $\kappa^2$ , leads to the most relevant Förster radii in the order of 7 nm for transfer along a channel. The value is 5.5 nm for vertical transfer to a chromophore in one of the six surrounding nearest neighbor channels. This means that all Förster radii of relevance lie between the values of  $R_0(\kappa^2=4)$  and  $R_0(\kappa^2=1)$ , as reported in Table 3.<sup>[61]</sup> These are very favorable values for the construction of efficient three-dye antenna composites of type c (Scheme 1). The average distance between the centers of adjacent tb-DXP molecules in a ZL channel at a loading,  $p$ , of 0.5 is 6 nm, and the distance between the centers of two channels is 1.84 nm thus very efficient FRET can occur. To test this experimentally, we prepared and analyzed the following composites: DMP,HR-ZL, DMP,tb-DXP-ZL, tb-DXP,HR-ZL, and DMP,tb-DXP,HR-ZL. Spectra of these samples are shown in Figures 8 and 9. The excitation spectrum of the DMP,HR-ZL sample in Figure 8A shows that the sensitivity below  $\lambda=450$  nm is con-

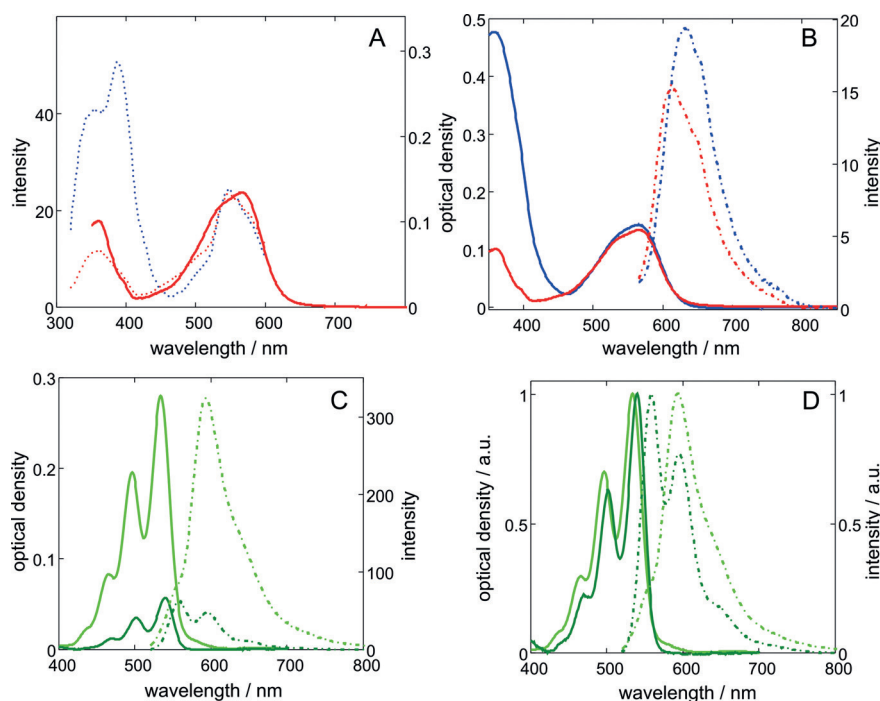


**Figure 8.** Absorption (—), fluorescence (---), and excitation (.....) spectra of dye-ZL composites. The fluorescence spectra were measured upon excitation at  $\lambda=490$  nm and the excitation spectra were observed at  $\lambda=690$  nm. A) Absorption and excitation spectrum of HR-ZL.04(0.5 IMZ<sup>+</sup>) (red), and excitation spectrum of DMP,HR-ZL.04,.15(0.5 IMZ<sup>+</sup>) (blue). B) Absorption and fluorescence spectra of HR-ZL.04(0.5 IMZ<sup>+</sup>) (red) and DMP,HR-ZL.04,.15(0.5 IMZ<sup>+</sup>) (blue). C) Comparison of the absorption (—) and fluorescence (---) spectra of tb-DXP-ZL.02 (green) and tb-DXP,HR-ZL.04,.27(0.5 IMZ<sup>+</sup>). D) Spectra from C) have been scaled to the same value at their respective maxima.

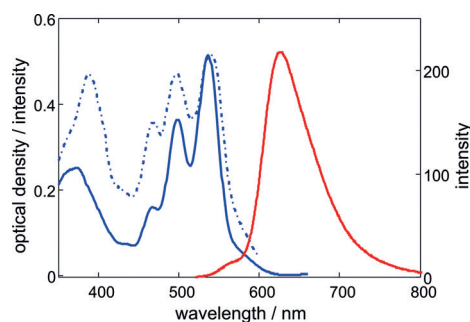


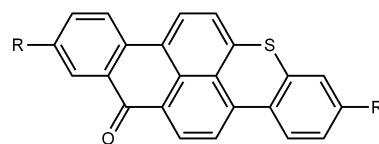
**Figure 9.** Three-color antenna system DMP,tb-DXP,HR-ZL<sub>TS-04,27,15</sub>(0.5IMZ<sup>+</sup>). Blue —, absorption; blue - - -, excitation, observed at  $\lambda = 680$  nm; red —, fluorescence excited at  $\lambda = 360$  nm.

siderably enhanced by the addition of DMP, and Figure 8B indicates that the shapes of the HR absorption and the fluorescence spectra are not affected. The results in Figure 8A and B demonstrate that energy transfer from DMP to HR is significant without the addition of tb-DXP. The spectra in Figure 8C and D demonstrate excellent energy-transfer efficiency from tb-DXP to HR in the tb-DXP,HR-ZL composite. The fluorescence quantum yields of optimized samples of this type are often larger than 80%.<sup>[30]</sup>

These two observations form the basis for understanding the remarkable antenna properties we have observed in DMP,tb-DXP,HR-ZL composites illustrated in Figure 9. The shape of the fluorescence band, observed under excitation at  $\lambda = 360$  nm corresponds to that of HR, with a small feature at shorter wavelength due to the tb-DXP. The band looks identical under excitation at  $\lambda = 490$  nm. The excitation spectrum, observed at  $\lambda = 680$  nm, follows the absorption spectrum. Interestingly, the intensity of the short-wavelength contribution, mainly stemming from the absorption of DMP, is larger than expected. This is probably caused by the scattering contribution at short wavelength, which is much lower in the range of emission of the HR acceptor. The essential conditions for obtaining highly luminescent composites with HR as the acceptor are that 1) 0.5 of the 3.6 exchangeable potassium cations per u.c. of ZL are substituted by IMZ<sup>+</sup>, and 2) HR is located in the middle of the channels, and thus, embedded between tb-DXP molecules, where it essentially feels the environment of the aliphatic tb tails.

Substituting one potassium cation per u.c. with IMZ<sup>+</sup> leads to the same result, whereas adding more IMZ<sup>+</sup> may cause problems because it starts to occupy too much of the available space in the channels.

Although most PDIs, and also HR and DMP, support insertion temperatures of 260 °C under vacuum conditions, IMZ<sup>+</sup> decomposes above about 200 °C, and thus damages the dye-ZL composites. The necessarily lower insertion temperature prolongs the synthetic procedure. PDIs that seem to travel more easily inside the channels (e.g., tb-DXP) are therefore of special interest. Organic cations other than IMZ<sup>+</sup>, such as those used by Li et al. to modify Laponite,<sup>[70]</sup> could be tested for fine-tuning the synthetic conditions and properties of the dye-ZL composites. The observation that the acceptor HR should be



**Scheme 8.** HR with substituents at the extremities of the long axis.

in the middle of the channels, which means that only organizational patterns b and c lead to strongly luminescent antenna composites, does not apply for cationic dyes such as oxonine and oxazine 1. However, these have so far, however, resulted in thermally less stable composites.<sup>[23]</sup> It appears to be worthwhile to test whether modified HR dyes (R,R'-HR; Scheme 8) substituted with appropriate R groups would allow inversion of the organization.

## Conclusion

Sequential insertion of different dyes into the 1D channels of ZL leads to sandwich structures, and thus allows the formation of sophisticated antenna composites for light harvesting, transport, and trapping. The basic concepts of dye alignment in 1D channel systems can, in principle, be applied to other zeolite framework types, such as AlPO<sub>4</sub>-5, and is also applicable to mesoporous materials.<sup>[71]</sup> Armbruster et al. were able to resolve the crystal structure of such a dye-Mordenite composite,<sup>[72]</sup> and Mintova et al. stressed the importance of progress in zeolite synthesis to promote advanced applications.<sup>[73]</sup> More general aspects of host-guest systems based on nanoporous crystals, including inorganic guests, have also been previously reported.<sup>[74]</sup> An important prerequisite for the integration of dye-loaded zeolites into devices, for example, for light-harvesting, is the availability of strategies for the synthesis of crystals with various well-defined sizes and aspect ratios. There has been substantial success in the field of tuning the size and aspect ratio of ZL crystals.<sup>[17-22]</sup> Furthermore, concepts for closing the channel entrances rely on the surface chemistry of silicates, thereby, so far, excluding aluminophosphate zeolites, such as AlPO<sub>4</sub>-5. This means that ZL remains the only host for which a synthetic strategy (Scheme 1) has been successful. Stopcock chemistry has recently, however, also been applied to metal-organic frameworks.<sup>[75]</sup>

Our synthetic procedures—from molecules and hosts to composite materials and composite-polymer matrices, including two- and three-color antennas—demonstrate the important flexibility of the strategy for creating a very promising class of composites with tunable spectroscopic and photo-physical properties. PDIs are important chromophores for the synthesis of artificial antenna systems and have therefore been considered in detail. The final step in the dye synthesis was, in general, a condensation reaction of a perylene precursor with the appropriate amines under high temperature and catalytic conditions. Therefore, the main challenge was the preparation of the corresponding amines. Of the 17 PDIs tested, 11 could be easily inserted into the ZL channels at elevated temperatures, 2 entered more reluctantly, and 4 could not be inserted

at all. The pattern we have observed improves phenomenological understanding considerably, so that results become more predictable, which enhances the possibilities for designing desired functionality. Controlling the substitution pattern of inserted dyes not only allows monitoring of the contact distance between nearest neighbors (so that, e.g., exciton interaction can be switched on and off), but also fine-tuning of transport properties, as well as altering the nanochannel environment. The fact that composites bearing reasonably good characteristics can be prepared with commercial zeolite underlines the usefulness of ZL as a host material. However, if purity, morphology, particle size, and particle size distribution matter, then it is advantageous to use well-described and reproducible published synthetic procedures. Sealing the channel entrances, so that the dye molecules cannot exit, is a prerequisite for achieving long-term stability of dye-ZL composites. We have shown that a variety of procedures can be used successfully. Plugging the channels, for example, with APTES is sufficient for sealing the channels against dye leakage. However, it does not prevent small molecules (such as acetonitrile, ethanol, water and oxygen) from entering and exiting the channels. As a result, the photochemical stability of the material, in particular, may be severely affected. Long-term photostability is an important issue for LSC devices. Sealing against smaller molecules is possible, for example, with the two imidazolium stopcocks we have reported as examples. Thus, we conclude that this route can be extended by designing specialized stopcocks for fine-tuning to achieve the desired properties. Embedding the ZL particles in a polymer matrix to obtain transparent layers can also be difficult because of their tendency to agglomerate. Composites sealed with APTES are much easier to disperse in PMMA films than unsealed ones. Additional modification of the coat with C18TES further improves this quality. Our results deepen our understanding of these systems extensively and facilitate the rational design of advanced dye-zeolite composite materials, which are of great interest as smart composites for LSCs in optoelectronics, sensing, and diagnostics. We provide powerful tools for further developing and understanding artificial antenna systems, which are among the most fascinating subjects of current photochemistry and photophysics.

## Experimental Section

### General

The synthesis of the dye-ZL composites consists of several steps outlined in this section. An extension of the experimental details is given in the Supporting Information. Some samples have been prepared by using commercially available ZL. This is indicated by adding TS as an index [e.g., dye1,dye2-ZL<sub>TS</sub>.05,.12(0.5IMZ<sup>+</sup>)].

### Synthesis of dyes

Details of the synthesis of the dyes can be found in the Supporting Information.

## Synthesis and postsynthetic treatment of ZL (LTL type)

The ZL crystals used in most of the experiments performed in this study were of barrel-type with a length and diameter of about 500 nm. Such crystals had a length that could accommodate a maximum of about 166 dye molecules per channel if each dye occupied 4 u.c.s. This made it possible to prepare dye-ZL composites with high light absorption capabilities, while the channel length was still short enough to keep the time required for diffusion processes short. The ZL crystals were synthesized by following a reported procedure.<sup>[20]</sup> However, we also tested to what extent commercial ZL materials, such as HSZ-500 from TOSOH Corporation (type HSZ-500 KOA, length  $\approx$ 400 nm, width  $\approx$ 500 nm) could be used. Commercial materials do not feature well-defined morphologies and may contain larger amounts of amorphous particles and cations other than K<sup>+</sup>.

SEM images of self-synthesized ZL and of commercial ZL from TOSOH Corporation used herein are shown in Figure 10. In both cases, it was necessary to perform a postsynthesis cation exchange with KNO<sub>3</sub> to ensure that the composition of the charge-compensating ions of the ZL was well defined (see the Supporting Information for more details).

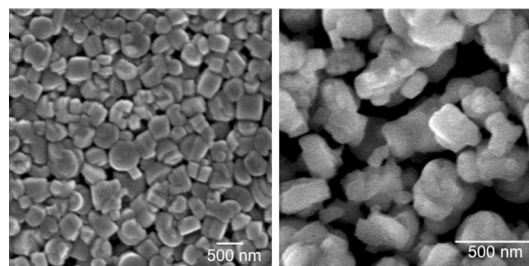


**Figure 10.** SEM images of ZL used in this study. Left: Self-synthesized (ZL). Right: Commercial HSZ-500KOA, TOSOH Corporation (ZL<sub>TS</sub>).

## Synthesis of dye-ZL composites

Depending on their nature, organic dyes were inserted into the channels of ZL either by ion exchange or through an adsorption process. Cationic species were incorporated into ZL by first dispersing the host material in an appropriate solvent, such as deionized water. The required amount of dye was then added to the ZL suspension as a stock solution, usually dissolved in the same solvent. Ion exchange was carried out either at room temperature or under gentle heating to increase the reaction rate. However, one had to be careful when heating the dye-containing ZL dispersion because the organic molecules could decompose if the exchange conditions were too harsh. The critical temperature regime depended very much on the kind of dyes used and on the conditions. An example of this behavior was the cationic dye oxazine 1 (Ox1<sup>+</sup>). If the ion-exchange process was carried out at a temperature above 70 °C, most of the dye decomposed, and only very small loadings could be achieved. Performing the same procedure at room temperature or 40 °C led to higher Ox1<sup>+</sup> loadings because the dye did not decompose under these conditions.<sup>[23]</sup> Neutral dyes were inserted into the ZL channels through adsorption in an evacuated and heated ampoule. In this process, the appropriate amount of dye was first adsorbed on the outer surface of the ZL by dispersing the host material in a solution of dye (see the Supporting Information).

## Plugging of channel entrances and modification of the surface

**Plugging of channel entrances:** Condensation of alkoxy silanes with the ZL silanol groups was used to modify the ZL coat and channel entrances. In such a condensation reaction, which could be carried out in a large variety of solvents, the alkoxy silane would bind to a surface Si–O–H group of the ZL under elimination of an alcohol, R–OH. A tertiary amine was used to catalyze the reaction. The ZL channel entrances were sealed by binding APTES to the composite. In a typical experiment, the dye–ZL composite (400 mg) was dispersed in toluene (70 mL) by means of a rotor/stator dispersion tool (Ultra Turrax T18 basic, IKA) for 20 min at 16000 rpm. Once the ZL was well dispersed, APTES (51  $\mu$ L) was added to the suspension. The condensation reaction was then carried out at room temperature for 3 h under constant treatment with the dispersion tool. The reacted material was then centrifuged (15 min at 2100 rpm) and washed twice with toluene. The material was then dried in a vacuum oven at 60 °C overnight (16 h). The molecular structures of the imidazole-containing stoppers (MelmiSil and BulmiSil) are given in Table 4. Both compounds were prepared according to procedures reported in ref. [76]. The experimental protocol to introduce the imidazolium stopcocks was similar to that of the sealing experiment with APTES. Sealing was tested in a leaking experiment, in which the treated and untreated HR–ZL composites were dispersed in a solution of 1-butanol/acetonitrile (1:1) and stirred at room temperature for 8 h. To ensure a good dispersion, as well as to test the effectiveness of the stopcock, the mixture was sonicated for 1 h. The suspension was then centrifuged for 15 min at 2100 rpm and the supernatants were filtered over a 0.22  $\mu$ m PTFE syringe filter to remove any residual small ZL particles. The amount of leaked dye was then determined by measuring the UV/Vis spectrum of the filtered supernatant. The samples were stored in transparent glass bottles at room temperature and normal light exposure.

**Surface modifications:** The surface of some APTES-modified dye–ZL composites was further functionalized by grafting additional types of alkoxy silanes. The sealing procedure described above left some unreacted ZL silanol and alkoxy silane groups. These could be used for additional condensation reactions with molecules such as MPTMS, CPTES, and C18TES (Table 4). For example, C18TES was successfully bound to an APTES-modified dye–ZL composite by first dispersing the material (170 mg) in toluene (70 mL) for 20 min at 16000 rpm by using the dispersion tool. Then C18TES (200  $\mu$ L) was added to the suspension, before stirring the mixture for 3 h at room temperature with the dispersion tool at 16000 rpm. The product was collected through centrifugation (15 min at 2100 rpm) and washed twice with toluene before being dried in a vacuum oven at 60 °C for 16 h.

## Embedding into PMMA and preparation of layers

An alternative to using OGS<sup>[23]</sup> to record absorption or emission spectra of dye–ZL composites were thin ZL-doped PMMA films. The refractive index of PMMA was very close to that of the dye–ZL composites, so that light scattering from non-agglomerated ZL particles could be minimized. Such thin films were prepared by first dispersing the sealed dye–ZL composite in an appropriate solvent, such as toluene or 1-butanol. This suspension was then added to a solution of PMMA in toluene or acetonitrile and mixed well. The best mixing results were obtained by using a rotor/stator dispersion tool. The films were then prepared by either casting in a Petri dish or depositing on a glass substrate with a film applicator

(Elcometer K3505). In the case of film casting, the solution of PMMA in toluene had a concentration of 100 mg mL<sup>-1</sup> PMMA, and the amount of dye–ZL composite used was 1 mg per 100 mg of PMMA (1 wt%). A more concentrated solution of PMMA was needed when using the film applicator. A 30 wt% solution in a 1:1 mixture of 1-butanol and acetonitrile, along with 1 wt% concentration of ZL, provided the best results when depositing films on glass substrates. The film applicator was set to deposit layers with a wet thickness of 250  $\mu$ m, which corresponded to films with a thickness of 100  $\mu$ m after drying and shrinking.

## Acknowledgements

Financial support by the Swiss Commission for Technology and Innovation (KTI/CTI, Project 12902.1 PFNM-NM) and the Schweizerische Bundesamt für Energiewirtschaft BFE (no. SI/500995-01) is gratefully acknowledged.

**Keywords:** dyes/pigments · FRET · host–guest systems · supramolecular chemistry · zeolites

- [1] G. Calzaferri, S. Huber, H. Maas, C. Minkowski, *Angew. Chem. Int. Ed.* **2003**, *42*, 3732–3558; *Angew. Chem.* **2003**, *115*, 3860–3888.
- [2] A. Bertucci, H. Lülfi, D. Septiadi, A. Manicardi, R. Corradini, L. De Cola, *Adv. Healthcare Mater.* **2014**, *3*, 1812–1817.
- [3] a) N. S. Kehr, S. Atay, B. Ergün, *Macromol. Biosci.* **2015**, *15*, 445–463; b) S. Hashimoto, *J. Phys. Chem. Lett.* **2011**, *2*, 509–519; c) D. Brühwiler, G. Calzaferri, T. Torres, J. H. Ramm, N. Gartmann, L.-Q. Dieu, I. López-Duarte, M. V. Martínez-Díaz, *J. Mater. Chem.* **2009**, *19*, 8040–8067; d) M. Pauchard, S. Huber, R. Méallet-Renault, H. Maas, R. Pansu, G. Calzaferri, *Angew. Chem. Int. Ed.* **2001**, *40*, 2839–2842; *Angew. Chem.* **2001**, *113*, 2921–2924.
- [4] N. Vilaça, R. Amorim, A. F. Machado, P. Parpot, M. F. R. Pereira, M. Sardo, J. Rocha, A. M. Fonseca, I. C. Neves, F. Baltazar, *Colloids Surf. B* **2013**, *112*, 237–244.
- [5] M. Tsotsalas, K. Kopka, G. Luppi, S. Wagner, M. P. Law, M. Schäfers, L. De Cola, *ACS Nano* **2010**, *4*, 342–348.
- [6] F. Cucinotta, A. Guenet, C. Bizzarri, W. Mróz, Ch. Botta, B. Milián-Medina, J. Gierschner, L. De Cola, *ChemPlusChem* **2014**, *79*, 45–57.
- [7] a) A. Mech, A. Monguzzi, F. Meinardi, J. Mezyk, G. Macchi, R. Tubino, *J. Am. Chem. Soc.* **2010**, *132*, 4574–4576; b) P. Cao, Y. Wang, H. Li, X. Yu, *J. Mater. Chem.* **2011**, *21*, 2709–2714; c) T. Wen, W. Zhang, X. Hu, L. He, H. Li, *ChemPlusChem* **2013**, *78*, 438–442.
- [8] R. N. Mahato, H. Lülfi, M. H. Siekman, S. P. Kersten, P. A. Bobbert, M. de Jong, L. De Cola, W. G. van der Wiel, *Science* **2013**, *341*, 257–260.
- [9] A. L. Gigli, R. Arletti, G. Tabacchi, E. Fois, J. Vitillo, G. Martra, G. Agostini, S. Quartieri, G. Vezzali, *J. Phys. Chem. C* **2014**, *118*, 15732–15743.
- [10] B. Schulte, M. Tsotsalas, M. Becker, A. Studer, L. De Cola, *Angew. Chem. Int. Ed.* **2010**, *49*, 6881–6884; *Angew. Chem.* **2010**, *122*, 7033–7036.
- [11] J. M. Beierle, R. Roswanda, P. M. Erne, A. C. Coleman, W. R. Browne, B. L. Feringa, *Part. Part. Syst. Charact.* **2013**, *30*, 273–279.
- [12] a) S. Hashimoto, M. Hagiri, N. Matsubara, S. Tobita, *Phys. Chem. Chem. Phys.* **2001**, *3*, 5043–5051; b) B. Bussemer, I. Dreiling, U. W. Grummt, G. J. Mohr, *J. Photochem. Photobiol. A* **2009**, *204*, 90–95.
- [13] G. Schulz-Ekloff, D. Wöhrle, B. van Duffel, R. A. Schoonheydt, *Microporous Mesoporous Mater.* **2002**, *51*, 91–138.
- [14] Ch. Sprung, B. Weckhuysen, *J. Am. Chem. Soc.* **2015**, *137*, 1916–1928.
- [15] O. Bossart, L. De Cola, S. Welter, G. Calzaferri, *Chem. Eur. J.* **2004**, *10*, 5771–5775.
- [16] I. López-Duarte, L.-Q. Dieu, I. Dolamic, M. V. Martínez-Díaz, T. Torres, G. Calzaferri, D. Brühwiler, *Chem. Eur. J.* **2011**, *17*, 1855–1862.
- [17] P. Li, Y. Wang, H. Li, G. Calzaferri, *Angew. Chem. Int. Ed.* **2014**, *53*, 2904–2909; *Angew. Chem.* **2014**, *126*, 2948–2953.
- [18] T. Ohsuna, B. Slater, F. Gao, J. Yu, Y. Sakamoto, G. Zhu, O. Terasaki, D. Vaughan, S. Qiu, C. Catlow, *Chem. Eur. J.* **2004**, *10*, 5031–5040.
- [19] O. Larlus, V. P. Valtchev, *Chem. Mater.* **2004**, *16*, 3381–3389.

- [20] A. Zabala Ruiz, D. Brühwiler, T. Ban, G. Calzaferri, *Monatsh. Chem.* **2005**, *136*, 77–89.
- [21] A. I. Lupulescu, M. Kumar, J. D. Rimer, *J. Am. Chem. Soc.* **2013**, *135*, 6608–6617.
- [22] T. Ban, M. Takamura, M. Morikawa, Y. Ohya, *Mater. Chem. Phys.* **2013**, *137*, 1067–1072.
- [23] A. Devaux, G. Calzaferri, I. Miletto, P. Cao, P. Belser, D. Brühwiler, O. Khorev, R. Häner, A. Kunzmann, *J. Phys. Chem. C* **2013**, *117*, 23034–23047.
- [24] A. Zabala Ruiz, H. Li, G. Calzaferri, *Angew. Chem. Int. Ed.* **2006**, *45*, 5282–5287; *Angew. Chem.* **2006**, *118*, 5408–5413.
- [25] K. B. Yoon, *Acc. Chem. Res.* **2007**, *40*, 29–40.
- [26] F. Cucinotta, Z. Popovic', E. A. Weiss, G. M. Whitesides, L. De Cola, *Adv. Mater.* **2009**, *21*, 1142–1145.
- [27] S. Hashimoto, K. Samata, T. Shoji, N. Taira, T. Tomita, S. Matsuo, *Microporous Mesoporous Mater.* **2009**, *117*, 220–227.
- [28] Y. Wang, H. Li, Y. Feng, H. Zhang, G. Calzaferri, T. Ren, *Angew. Chem. Int. Ed.* **2010**, *49*, 1434–1438; *Angew. Chem.* **2010**, *122*, 1476–1480.
- [29] S. Fibikar, G. Luppi, V. Martínez-Junza, M. Clemente-Léon, L. De Cola, *ChemPlusChem* **2015**, *80*, 62–67.
- [30] A. Devaux, G. Calzaferri, P. Belser, P. Cao, D. Brühwiler, A. Kunzmann, *Chem. Mater.* **2014**, *26*, 6878–6885.
- [31] M. Busby, A. Devaux, C. Blum, V. Subramaniam, G. Calzaferri, L. De Cola, *J. Phys. Chem. C* **2011**, *115*, 5974–5988.
- [32] G. Calzaferri, D. Brühwiler, T. Meng, L.-Q. Dieu, V. L. Malinovskii, R. Häner, *Chem. Eur. J.* **2010**, *16*, 11289–11299.
- [33] M. Busby, C. Blum, M. Tibben, S. Fibikar, G. Calzaferri, V. Subramaniam, L. De Cola, *J. Am. Chem. Soc.* **2008**, *130*, 10970–10976.
- [34] G. Calzaferri, K. Lutkouskaya, *Photochem. Photobiol. Sci.* **2008**, *7*, 879–910.
- [35] E. Fois, G. Tabacchi, G. Calzaferri, *J. Phys. Chem. C* **2010**, *114*, 10572–10579.
- [36] a) Th. Förster, *Naturwissenschaften* **1946**, *33*, 166–175; b) Th. Förster, *Ann. Phys.* **1948**, *437*, 55–75.
- [37] M. Pauchard, A. Devaux, G. Calzaferri, *Chem. Eur. J.* **2000**, *6*, 3456–3470.
- [38] a) T. Weil, T. Vosch, J. Hofkens, K. Peneva, K. Müllen, *Angew. Chem. Int. Ed.* **2010**, *49*, 9068–9072; *Angew. Chem.* **2010**, *122*, 9252–9278; b) D. Jänsch, C. Li, L. Chen, M. Wagner, K. Müllen, *Angew. Chem. Int. Ed.* **2015**, *54*, 2285–2289; *Angew. Chem.* **2015**, *127*, 2314–2319.
- [39] H. Bittermann, D. Siegemund, V. L. Malinovskii, R. Häner, *J. Am. Chem. Soc.* **2008**, *130*, 15285–15287.
- [40] C. B. Winiger, S. M. Langenegger, G. Calzaferri, R. Häner, *Angew. Chem. Int. Ed.* **2015**, *54*, 3643–3647.
- [41] a) International Zeolite Association, <http://www.iza-structure.org>; b) Ch. Baerlocher, L. B. McCusker, D. H. Olson, *Atlas of Zeolite Framework Types*, 6th ed., Elsevier, Amsterdam, **2007**.
- [42] C. Marcolli, G. Calzaferri, *Appl. Organomet. Chem.* **1999**, *13*, 213–226.
- [43] IMZ<sup>+</sup>: 1-ethyl-3-methyl imidazolium chloride counterion.
- [44] M. Myahkostopov, V. Prusakova, D. G. Oblinsky, G. D. Scholes, F. N. Castellano, *J. Org. Chem.* **2013**, *78*, 8634–8638.
- [45] J. Liu, Y. Li, Y. Li, N. Hu, *J. Appl. Polym. Sci.* **2008**, *109*, 700–707.
- [46] B. L. Small, R. Rios, E. R. Fernandez, D. L. Gerlach, J. A. Halfen, M. J. Carney, *Organometallics* **2010**, *29*, 6723–6731.
- [47] R. Mishra, J. M. Lim, M. Son, P. Panini, D. Kim, J. Sankar, *Chem. Eur. J.* **2014**, *20*, 5776–5786.
- [48] H. Langhals, *Chem. Ber.* **1985**, *118*, 4641–4645.
- [49] F. Nolde, J. Qu, C. Kohl, N. G. Pschirer, E. Reuther, K. Müllen, *Chem. Eur. J.* **2005**, *11*, 3959–3967.
- [50] Y. Geerts, H. Quante, H. Platz, R. Mahrt, M. Hopmeier, A. Bohm, K. Müllen, *J. Mater. Chem.* **1998**, *8*, 2357–2369.
- [51] H. Quante, K. Müllen, *Angew. Chem. Int. Ed. Engl.* **1995**, *34*, 1323–1325; *Angew. Chem.* **1995**, *107*, 1487–1489.
- [52] T. Yamamoto, A. Morita, Y. Miyazaki, T. Maruyama, H. Wakayama, Z. H. Zhou, Y. Nakamura, T. Kanbara, S. Sasaki, K. Kubota, *Macromolecules* **1992**, *25*, 1214–1223.
- [53] W. Bradley, F. W. Pexton, *J. Chem. Soc.* **1954**, 4432–4435.
- [54] E. Fois, G. Tabacchi, A. Devaux, P. Belser, D. Brühwiler, G. Calzaferri, *Langmuir* **2013**, *29*, 9188–9198.
- [55] G. Calzaferri, A. Devaux, in *Supramolecular Photochemistry: Controlling Photochemical Processes* (Eds.: V. Ramamurthy, Y. Inoue), Wiley, Hoboken, **2011**, Chapter 9, pp. 285–387.
- [56] A. Rademacher, S. Märkle, H. Langhals, *Chem. Ber.* **1982**, *115*, 2927–2934.
- [57] a) J. S. Park, Y.-J. Lee, K. B. Yoon, *J. Am. Chem. Soc.* **2004**, *126*, 1934–1935; b) A. Kulak, Y.-J. Lee, Y. S. Park, K. B. Yoon, *Angew. Chem. Int. Ed.* **2000**, *39*, 950–953; *Angew. Chem.* **2000**, *112*, 980–983.
- [58] a) N. R. E. N. Impens, P. van der Voort, E. F. Vansant, *Microporous Mesoporous Mater.* **1999**, *28*, 217–232; b) T. Kawai, K. Tsutsumi, *Colloid Polym. Sci.* **1998**, *276*, 992–996.
- [59] a) W. Xu, Q. Luo, H. Wang, L. C. Francesconi, R. E. Stark, D. L. Akins, *J. Phys. Chem. B* **2003**, *107*, 497–501; b) N. K. Mal, M. Fujiwara, Y. Tanaka, *Nature* **2003**, *421*, 350–353; c) J. Liu, X. Feng, G. E. Fryxell, L.-Q. Wang, A. Y. Kim, M. Gong, *Adv. Mater.* **1998**, *10*, 161–165.
- [60] T. Ban, D. Brühwiler, D. Calzaferri, *J. Phys. Chem. B* **2004**, *108*, 16348–16352.
- [61] G. Calzaferri, *Langmuir* **2012**, *28*, 6216–6231.
- [62] A. Guerrero-Martínez, S. Fibikar, I. Pastoriza-Santos, L. M. Liz-Marzán, L. De Cola, *Angew. Chem. Int. Ed.* **2009**, *48*, 1266–1270; *Angew. Chem.* **2009**, *121*, 1292–1296.
- [63] Y. Wang, Y. Yue, H. Li, Q. Zhao, Y. Fang, P. Cao, *Photochem. Photobiol. Sci.* **2011**, *10*, 128–132.
- [64] G. Tabacchi, E. Fois, G. Calzaferri, *Angew. Chem. Int. Ed.* **2015**, *54*, 11112–11116, *Angew. Chem.* **2015**, *127*, 11264–11268.
- [65] a) S. Suárez, A. Devaux, J. Bañuelos, O. Bossart, A. Kunzmann, G. Calzaferri, *Adv. Func. Mater.* **2007**, *17*, 2298–2306; b) J. Schneider, D. Fanter, M. Bauer, C. Schomburg, D. Wöhrle, G. Schulz-Ekloff, *Microporous Mesoporous Mater.* **2000**, *39*, 257–263.
- [66] G. Griffini, L. Brambilla, M. Levi, M. Del Zoppo, S. Turri, *Sol. Energy Mater. Sol. Cells* **2013**, *111*, 41–48.
- [67] N. Tanaka, N. Barashkov, J. Heath, W. N. Sisk, *Appl. Optics* **2006**, *45*, 3846–3851.
- [68] L. Danos, T. J. Meyer, P. A. Kittidachan, L. Fang, T. S. Parel, N. Soleimani, T. Markvart, in *Materials Challenges: Inorganic Photovoltaic Solar Energy* (Ed. S. J. C. Irvine), RCS, Cambridge, **2015**, Chapter 9: *Photon Frequency Management Materials for Efficient Solar Energy Collection*, p. 297–331.
- [69] a) M. G. Debije, P. P. Verbunt, *Adv. Energy Mater.* **2012**, *2*, 12–35; b) T. Dienel, C. Bauer, I. Dolamic, D. Brühwiler, *Sol. Energy* **2010**, *84*, 1366–1369; c) J. C. Goldschmidt, M. Peters, A. Bösch, H. Helmers, F. Dimroth, S. W. Glunz, G. Willeke, *Sol. Energy Mater. Sol. Cells* **2009**, *93*, 176–182.
- [70] D. Yang, Y. Wang, Y. Wang, Z. Li, H. Li, *ACS Appl. Mater. Interfaces* **2015**, *7*, 2097–2103.
- [71] a) G. Ihlein, F. Schüth, O. Krauss, U. Vietze, F. Laeri, *Adv. Mater.* **1998**, *10*, 1117; b) T. H. Noh, H. Lee, J. Jang, O.-S. Jung, *Angew. Chem. Int. Ed.* **2015**, *54*, 9284–9288; *Angew. Chem.* **2015**, *127*, 9416–9420.
- [72] P. Simoncic, T. Armbruster, P. Pattison, *J. Phys. Chem. B* **2004**, *108*, 17352–17360.
- [73] M. Zaarour, B. Dong, I. Naydenova, R. Retoux, S. Mintova, *Microporous Mesoporous Mater.* **2014**, *189*, 11–21.
- [74] F. Laeri, F. Schüth, U. Simon, M. Wark, *Host–Guest Systems Based on Nanoporous Crystals*, Wiley-VCH, Weinheim, **2003**.
- [75] H. Wang, J. Xu, D.-S. Zhang, Q. Chen, R.-W. Wen, Z. Chang, X.-H. Bu, *Angew. Chem. Int. Ed.* **2015**, *54*, 5966–5971; *Angew. Chem.* **2015**, *127*, 6064–6068.
- [76] Y. Lu, S. S. Moganty, J. L. Schaefer, L. A. Archer, *J. Mater. Chem.* **2012**, *22*, 4066–4072.

Received: November 2, 2015

Published online on February 11, 2016